Multiband quasibound states in the continuum engineered by space-group-invariant metasurfaces

Ruoheng Chai,[1] Wenwei Liu,[1,*] Zhancheng Li,[1] Hua Cheng,[1,†] Jianguo Tian,[1] and Shuqi Chen[1,2,3,‡]

[1]*The Key Laboratory of Weak Light Nonlinear Photonics, Ministry of Education, Renewable Energy Conversion and Storage Center, School of Physics and TEDA Institute of Applied Physics, Nankai University, Tianjin 300071, China*

[2]*The Collaborative Innovation Center of Extreme Optics, Shanxi University, Taiyuan, Shanxi 030006, China*

[3]*Collaborative Innovation Center of Light Manipulations and Applications, Shandong Normal University, Jinan, Shandong 250358, China*

(Received 19 May 2021; revised 7 August 2021; accepted 10 August 2021; published 26 August 2021)

Bound states in the continuum (BICs) enabling resonances with high quality (Q) factor allow for high-efficiency light-matter interactions and boost various research fields such as nonlinear photonics and optical detecting. However, further improvement of the Q factor of the resonances is challenging since the accurate fabrication of the tiny symmetry defects of meta-atoms is limited by the nanofabrication technology, which is critical for transition from BICs to quasi-BICs in previous works. Here we propose a different approach to trigger the transition of quasi-BICs that does not need to change the space group symmetry of nanostructures. By modulating the periods of the nanostructures, our approach enlarges the unit cell and enriches the ideal BICs eigenstates, achieving multiband quasi-BICs in metasurfaces. By tuning the asymmetry parameters, the selective excitation of multiband quasi-BICs is demonstrated. Thanks to the multi-narrow-band resonances obtained by the unit cell perturbation, a multivariable sensing method is proposed to simultaneously obtain the birefringence property and thickness of a nanoscale layer. The proposed approach exciting multiband quasi-BICs offers a possible solution for ultra-high-Q devices without complex fabrication techniques and may found realistic application in many fields such as harmonic generation, optical detecting, and compact low-threshold lasers.

DOI: 10.1103/PhysRevB.104.075149

I. INTRODUCTION

Bound states in the continuum (BICs) are discrete eigenstates of open wave systems that are embedded in free-space radiation but completely orthogonal to the radiative continuum [1,2]. BICs are regarded as a universal wave phenomenon and have been extensively investigated in many research fields including electronics [3], acoustics [4], microwaves [5], and nanophotonics [6]. Recent advances in photonics reveal that some guided resonances could completely decouple from the radiative continuum, as a result of symmetry mismatch [7–9]. These radiative singularities were further identified as polarization vortices with integral topological charge [10]. One case of BICs is pinned at Γ point as long as the structure symmetry is invariant, known as "symmetry-protected BICs" [11–14]. Another type of BICs could relocate, merge, or annihilate in k space when tuning system parameters. These BICs are regarded as "accidental BICs" since they originate from accidental destructive interferences between different resonances [15,16]. Recently, the concept of BICs has boosted numerous applications in linear and nonlinear nanophotonics that leverage high-Q resonances and strong electromagnetic (EM) energy confinements at the nanoscale. For example, Liu *et al.* proposed that ellipticity modulation of linear polarization could be achieved based on pairs of circularly polarized states spawn from BICs [17]. Huang *et al.* demonstrated an ultrafast BICs laser with the switching time reaching picoseconds level [18]. Wang *et al.* proposed guided resonances near BICs as orientation-variant wave plates in the momentum space and achieved a direct optical vortex generator that does not require central alignment [19].

Symmetry breaking is a vital and intriguing phenomenon that is related to nontrivial effects in many physical processes [20]. For example, breaking lattice inversion symmetry can transform Dirac points to Weyl points [21] and nonreciprocal wave propagation can be achieved by breaking time-reversal symmetry [22]. BICs could be transformed into quasi-BICs and achieve ultra-high-Q resonances by tiny symmetry breaking of structures [11–14,23,24]. BICs result from the strong coupling between the resonant eigenstates in parameter space and appear as sharp Fano peaks (quasi-BICs) when they weakly couple to the radiative continuum [5,6,25–27]. By group theory analysis of eigenstate modes in momentum space, a road map was depicted for engineering far-field polarization of quasi-BICs [28]. Conventionally, nanostructures-based quasi-BICs mainly originate from in-plane or out-of-plane symmetry breaking of the building blocks. However, since the radiative Q factor of quasi-BICs is proportional to the power inversion of asymmetry parameters [14], Q factor is limited by certain geometric defects, leading to experimental challenges to realize the designed high Q factors [24]. On the other hand, the space group of these devices degenerates into its subgroup when introducing defects into meta-atoms. These defects simultaneously break the symmetry elements and the space group of structures.

*Corresponding author: wliu@nankai.edu.cn
†Corresponding author: hcheng@nankai.edu.cn
‡Corresponding author: schen@nankai.edu.cn

However, the exact relationship among the symmetry elements, space group, and the transition of quasi-BICs still needs to be investigated.

Metasurfaces are arrays of artificial subwavelength nanostructures that can sufficiently manipulate the EM fields at nanoscale [29]. With abundant local resonances enabled by the artificial nanostructures, such as Bragg resonances [30], Mie resonances [31,32], and surface plasmon polaritons [33], metasurfaces provide a versatile platform to realize holography, optical information multiplexing and possessing, and harmonic waves manipulation [34–38]. By combining the high Q nature of BICs and the EM fields manipulation of artificial nanostructures, the light-matter interaction efficiency of metasurfaces can be further enhanced, which can potentially lead to efficient applications in nonlinear and quantum physics. The ultra-high-Q resonances can be applied in various promising applications such as optical sensing and detecting since devices inspired by BICs have extremely high sensitivity and can achieve a lower detection threshold [39–41]. However, the current optical sensing methods are still limited to isotropic media, and to our knowledge, the anisotropic refractive index detection on the metasurfaces platform has not been explored yet. On the other hand, traditional resonance-shift-based sensing is not only affected by the refractive index of the media to be measured but also affected by environmental parameters such as temperature, cladding thickness, and surface roughness, which are challenging to be separated.

Here, we propose a multiband quasi-BICs transition method, which can realize the transition from ideal symmetry-protected BICs to quasi-BICs by breaking the symmetry elements of nanostructures and simultaneously identify the anisotropic refractive index and the thickness of a nanoscale layer. Different from previous works that require simultaneous symmetry breaking of meta-atoms and the space group to trigger the transition of quasi-BICs, we find that the out-coupling of BICs can be achieved by engineering the period of the metasurface, which changes specific symmetry elements (C_2 and σ) of the nanostructure while keeping the space group invariant (pmm). Such perturbation enlarges the unit cell and enriches the eigenstates of ideal BICs, achieving multiband quasi-BICs. It is noted that researchers have achieved other nontrial effects as well by enlarging the unit cell size of artificial microstructures, such as band inversion and topological edge states [42]. By tuning the asymmetry parameters in the x or y direction, a frequency-selective excitation of multiband quasi-BICs is achieved by different symmetries of eigenstate fields. Furthermore, the identification among birefringent refractive indices and cladding thickness can be realized based on the proposed quasi-BICs transition method.

II. DESIGN OF QUASI-BICS

The schematic of the proposed metasurface composed of silicon nanoboxes and a SiO_2 substrate is shown in Figs. 1(a) and 1(b). We consider four identical nanoboxes as the unit cell of our periodic planar structure. The gaps sizes g inside the unit cell in both x and y directions have the same value and remain invariant, which are fixed at $g = 120$ nm. The periods in x and y directions of the original metasurface are

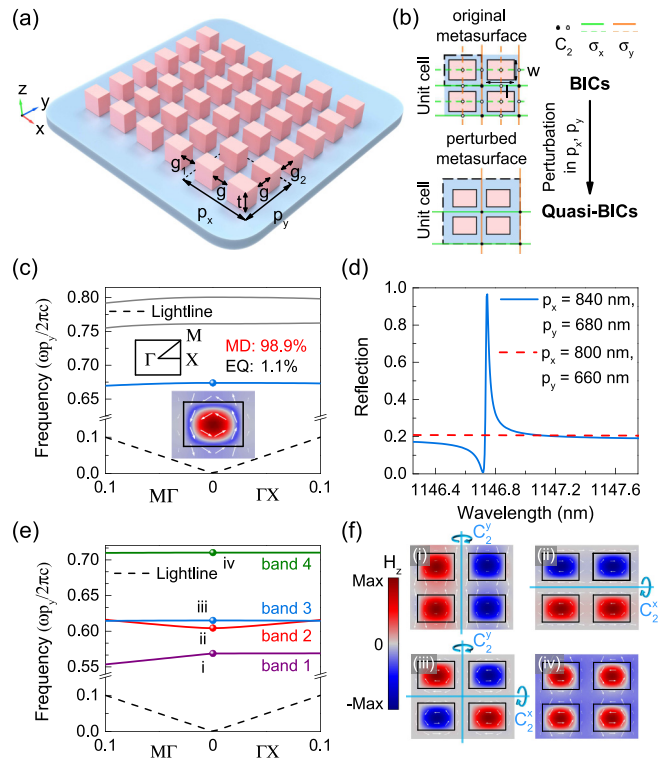

FIG. 1. (a) Schematic of a metasurface consisting of silicon nanoboxes. The length, width, and thickness of the nanoboxes are l, w, and t, respectively. The periods in the x and y directions are p_x and p_y. g is the neighboring gap among nanoboxes in the same unit cell, with g_1 and g_2 being the gap sizes between successive unit cells along the x and y directions, respectively. (b) The symmetry elements of the the original metasurface (upper panel) and the perturbed metasurface (lower panel). The dots indicate the fixed points of half turns (C_2) and lines represent axes of reflection (green lines for σ_x and orange lines for σ_y). Black dots and solid lines represent retained symmetry elements, while white dots and dashed lines indicate broken symmetry elements. (c) Lowest three bands supported by the original metasurface. Inset: the EM fields distribution of a single unit cell at Γ point, where the color depicts the z component of the magnetic field. (d) The reflection spectra of the original metasurface (red dashed line) and the perturbed metasurface (blue solid line), with a y-polarized incident plane wave. (e),(f) Band structure and corresponding EM fields distributions of the perturbed metasurface. The light blue lines are out-of-plane C_2 axes.

set as $p_x = 800$ nm and $p_y = 660$ nm. When the gap size meets the condition $g_1 = g_2 = g$, a single nanobox can also be considered as a unit cell. The refractive index of SiO_2 is set as 1.5 and the permittivity of Si in the near-infrared wavelengths is adopted from experimental data of Palik [43]. Conventionally, the transition from symmetry-protected BICs to quasi-BICs is triggered by introducing defects into meta-atoms which simultaneously breaks the symmetry elements and the space group of structures [11–14]. In our design, we can alternatively trigger the transition from BICs to quasi-BICs by perturbing the periods (p_x or p_y at around 800 nm and 660 nm, respectively) or the gap sizes (g_1 or g_2 at around 120 nm) for the perturbed metasurface. This kind of symmetry breaking does change symmetry elements of nanostructures

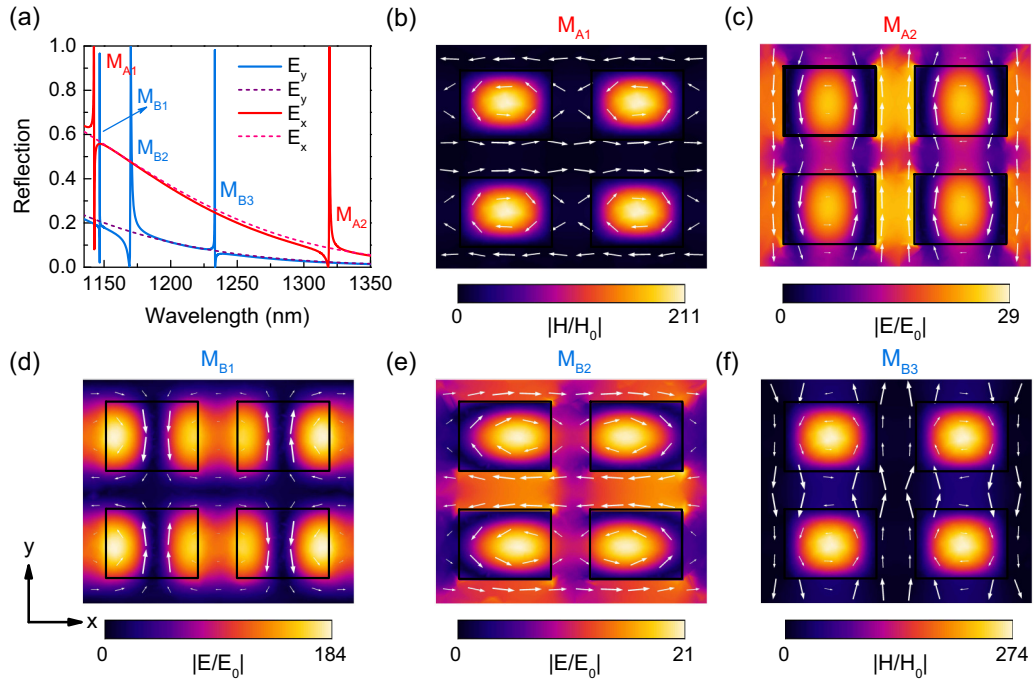

FIG. 2. Mode analysis of multiband quasi-BICs. (a) Reflection spectra of the original metasurface ($p_x = 800$ nm and $p_y = 660$ nm, solid lines) and the perturbed metasurface ($p_x = 820$ nm and $p_y = 680$ nm, dashed lines) by normal incident plane waves. E_i implies the incident polarization ($i = x,\ y$). (b),(c) EM fields distributions at different resonant modes (M_{A1}, M_{A2}) with x-polarized incident light. (d)–(f) EM fields distributions at different resonant modes (M_{B1}, M_{B2}, and M_{B3}) with y-polarized incident light. The EM fields are depicted in the x-y cutplane bisecting the nanoboxes and are normalized to the incident EM fields intensity. The color maps depict magnetic (electric) field enhancement for mode M_{A1}, and M_{B3} (M_{A2}, M_{B1}, and M_{B2}), and white arrows depict electric (magnetic) field.

such as half turns (C_2) pinned at the center of the nanobox (indicated by white dots) and mirror axes (σ_x and σ_y) connecting these C_2 points (dashed lines), while keeping the entire space group isomorphism invariant (*pmm*) [44]. The band diagram of the original metasurface is shown in Fig. 1(c). We focus on the lowest band shown as the blue line. To clearly show the origination of this band, the multipole contributions of the eigenstate field are analyzed [45]. We expand the scattering energy to the first four items, namely electric dipole (ED), magnetic dipole (MD), electric quadrupole (EQ), and magnetic quadrupole (MQ). The results show that nearly 99% of the scattering energy comes from MD. Combining the eigenstate field distribution in the inset of Fig. 1(c), we confirm that the MD oscillates along the z direction, which cannot be excited by a normally incident plane wave. Since the nondegenerate bound state at the Γ point resides in the radiation continuum, it is considered a BIC [46]. By merely breaking the aforementioned symmetry elements of the nanostructures, the radiation leakage of ideal BICs modes towards free space can be achieved, appearing as sharp Fano peaks as shown in Fig. 1(d) (one of the quasi-BICs resonances shown for simplicity).

As a result of perturbation on the periods, the eigenstates and ideal BICs are enriched. The eigenstate field at Γ point of the perturbed metasurface in Figs. 1(e) and 1(f) could be understood as bonding and antibonding hybridization of the characteristic resonant modes of the constituent nanoboxes, which is analogous to the plasmon hybridization [47]. The symmetries of resonant eigenstates correspond to irreducible representations of the C_{2v} point group, namely two antisymmetric B representations (for modes i and ii) and two symmetric A representation (for modes iii and iv), as shown in Fig. 1(f). Thus, ideal BICs modes can be theoretically enriched by four times for different hybridization of eigenstate field, achieving multiband quasi-BICs. The eigenstate field distributions shown in Fig. 1(f) also distinguish out-of-plane C_2 symmetries (C_2^x or C_2^y), and they are BICs protected by different symmetries. The bands and the eigenstate field distributions in this paper are obtained by finite-element-method (FEM) eigenvalue solver in COMSOL Multiphysics. The solver searches the eigenvalues around 300 THz. The relative computing errors of solutions are lower than 10^{-6}. We did not consider the effects of substrate in Fig. 1 to obtain the ideal dipole decomposition in theory. To show the ideal BICs, we set the same parameter values for the original and perturbed metasurfaces (g, g_1, and $g_2 = 120$ nm), except that the perturbed metasurface has a four times larger unit cell in the simulations.

III. RESULTS AND DISCUSSIONS

The perturbations of the periods ($p_x = 820$ nm, $p_y = 680$ nm) enable BICs to appear as ultrasharp Fano lineshapes, achieving multiband quasi-BICs excitation as shown in Fig. 2(a). The Fano lineshapes disappear when the disorders are removed. The quasi-BICs resonances of M_{Ai} ($i = 1,\ 2$) and M_{Bj} ($j = 1,\ 2,\ 3$) correspond to x- and y-polarized incident light, respectively. For the transverse electric (TE) mode in Fig. 2(b), mode M_{A1} consists of four MD modes oriented along the z direction, with in-phase (out-of-phase)

hybridizations in the x (y) direction. Similarly, mode M_{B3} plotted in Fig. 2(f) can be understood as hybridization of MD modes in the opposite way. The transverse magnetic (TM) modes M_{A2} and M_{B2} can be decomposed into in-phase and out-of-phase EDs as well [see Figs. 2(c) and 2(e)]. Different from the four modes discussed above, mode M_{B1} consists of four MDs along the y direction, oriented antiparallelly in both the x and y directions, as shown in Fig. 2(d). Besides, the electric field of resonance mode M_{B1} is mostly localized around the structure gap, and the normalized electric field amplitude $|E/E_0|$ is enhanced by more than 10^2 times,which is desirable for applications such as optical sensing and harmonic generation.

Along with symmetry breaking, BICs transform to quasi-BICs, leaking lights to free space and with Q factors decreasing drastically [14]. This is a typical characteristic of quasi-BICs and is important for realistic applications. The Fano lineshape evolutions as a function of asymmetry parameters p_x, p_y, or δp are demonstrated in Figs. 3(a)–3(e), where δp denotes the same perturbation of p_x and p_y deviated from 800 nm and 660 nm, respectively. The refection spectra show that the linewidths of these five peaks expand wider for larger asymmetry parameters. The narrow lineshapes will disappear if the symmetry disorder is zero, indicating ideal BICs. Additionally, the linear-polarized plane waves can selectively stimulate quasi-BICs modes M_{A1} and M_{B2} by only tuning p_y [see dashed lines in Fig. 3(f)]. The modes M_{A2} and M_{B3} could be selectively excited by x- or y-polarized incident lights by only changing p_x [see solid lines in Fig. 3(f)]. In the case of perturbating both p_x and p_y, all five quasi-BICs modes could be excited by linear-polarized incident light, as aforementioned in Fig. 2(a). Thus, selective excitation of multiband quasi-BICs can be achieved by tuning one or two asymmetry parameters.

To explain the selective excitation effects, we further investigate the free-space-coupling behaviors of BICs when tuning asymmetry parameters as shown in Fig. 4. We take mode M_{A1}, M_{A2}, and M_{B1} as examples. One of the intuitive physical quantities to estimate free-space out-coupling is the radiative Q factor of resonances. As shown in Figs. 4(a)–4(c), we simulated the two-dimensional (2D) maps of the Q factor as a function of both p_x and p_y [$Q(p_x, p_y)$]. The Q factors are derived from calculated complex eigenfrequencies of the modes using FEM. We can see their different behaviors, which are consistent with the selective excitation in spectra in Fig. 3. For the BICs mode M_{A1} shown in Fig. 4(a), p_x barely affects its Q factor while the Q factor drastically decreases when p_y deviates from 660 nm (the parameter value of the original metasurface). For the mode M_{A2}, the effects of p_x and p_y will exchange. For the mode M_{B1}, we could only trigger the transition from BICs to quasi-BICs by simultaneously modulating p_x and p_y. The ultra-high-Q pale yellow regions in Figs. 4(a)–4(c) depict different BICs shapes, indicating that symmetry breaking requires different asymmetry parameters in these ideal BICs modes.

The out-of-phase hybridization of modes brings in distinct symmetries. In Figs. 4(d)–4(f) we illustrate the eigenstate fields of BICs corresponding to modes M_{A1}, M_{A2}, and M_{B1}. For mode M_{A1}, as long as the out-of-phase condition is satisfied, the MD radiations will be perfectly canceled in the far field through destructive interferences, forming symmetry-protected BICs. It is noted that the out-of-phase hybridization introduces out-of-plane C_2 axes along the x direction (C_2^x) in the x-y eigenstate fields cutplane. Thus, merely perturbating p_x does not break the symmetry elements and could not trigger the transition of quasi-BICs. Similarly, BICs mode M_{A2} possesses out-of-plane C_2 axes along the y direction (C_2^y). The effects of p_y and p_x exchange for mode M_{A2}. BICs mode M_{B1} owns out-of-plane C_2 axes in both x and y directions (C_2^x and C_2^y). We can transform BICs mode M_{B1} to quasi-BICs by simultaneously breaking symmetry elements C_2^x and C_2^y. Such relationship between symmetry and quasi-BICs transition demonstrates that the selective excitation of quasi-BICs is

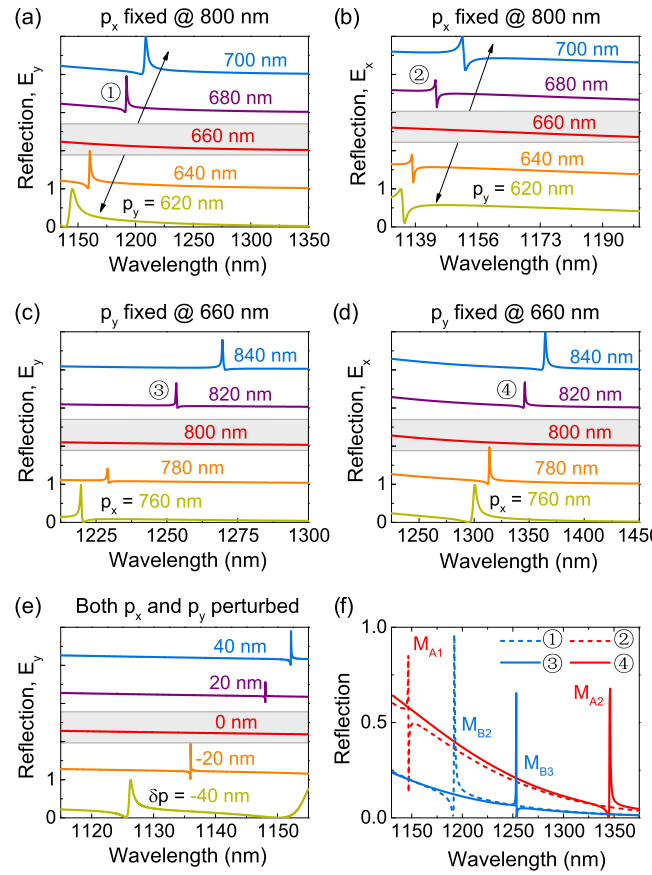

FIG. 3. Fano lineshapes evolution versus asymmetry parameters and selective excitation of multiband quasi-BICs. (a),(b) Reflection spectra of designed metasuface as a function of p_y with y- and x-polarized incidence, where $p_x = 800$ nm. The black arrows are an eye guide to show the degree of symmetry breaking and the gray regions represent the original metasurface. (c),(d) Reflection spectra of the perturbed metasurface as a function of p_x with y- and x-polarized incidence, where $p_y = 660$ nm. (e) Reflection spectra of the perturbed metasurface as a function of δp with y-polarized incident plane waves. Note that this case is the same as Fig. 2(a), which means all five quasi-BICs modes could appear if both p_x and p_y are perturbed. (f) Reflection spectra in the case of ①-④ with larger wavelength range, to show clearly that only one quasi-BIC can be excited in the operating spectral region by x- or y-polarized plane waves.

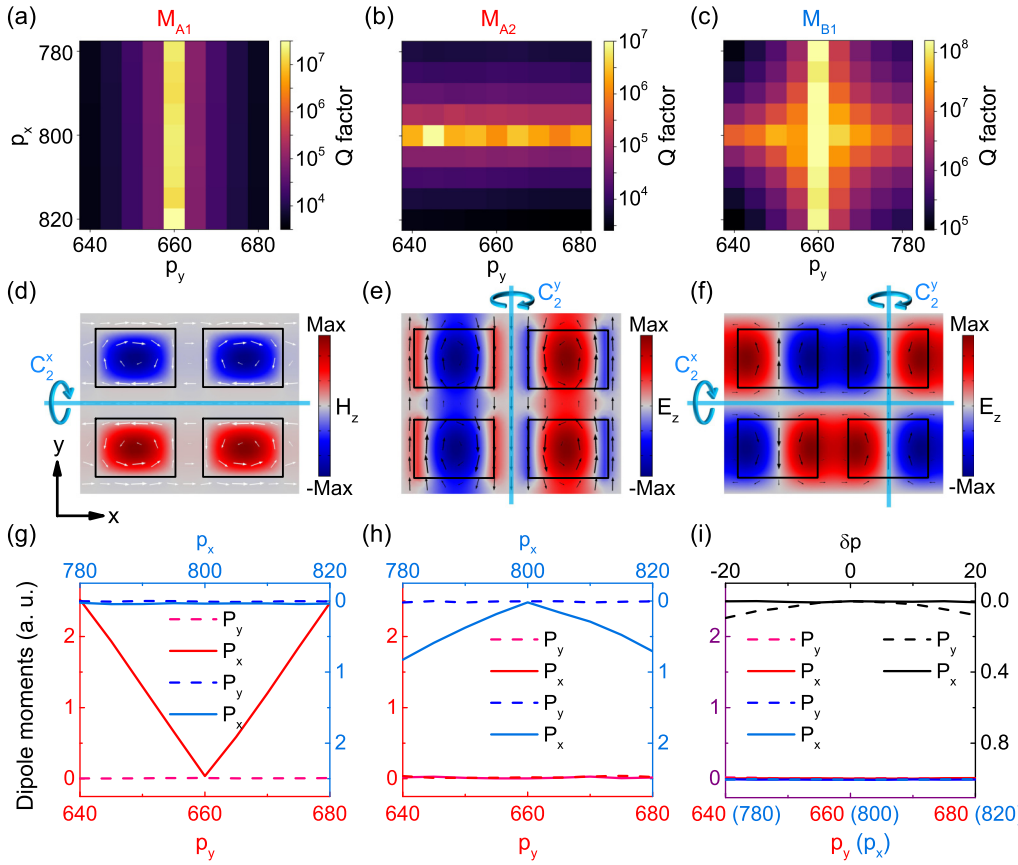

FIG. 4. Eigenmode calculation and coupling strength analysis by in-plane ED moment. (a)–(c) Q factor maps of BICs mode M_{A1}, M_{A2}, and M_{B1} supported by designed metasuface as a function of p_x and p_y. (d)–(f) EM fields distributions of eigenmode M_{A1}, M_{A2}, and M_{A3} supported by the original metasurface. Out-of-plane components of EM fields are plotted as color maps and the corresponding in-plane components are depicted by arrows (white arrows for TE modes and black for TM modes). Light blue lines represent out-of-plane half turns C_2^x and C_2^y. (g)–(i) In-plane ED moment components P_x (solid lines) and P_y (dashed lines) versus asymmetry parameters p_x (blue lines), p_y (red lines), and δp (black lines).

determined by the symmetry of eigenstate fields (irreducible representations).

To more quantitatively estimate eigenstate free-space outcoupling, one can employ the overlapping between incident wave field and eigenstate field. We assume $e^{-i\omega t}$ time dependence of EM fields and express the eigenstate field in the form of current density. The coupling strength c can be written as [48]:

$$c \propto \int_V [\mathbf{j}(\mathbf{r}) \cdot \mathbf{E}] e^{ikz}]\, d\mathbf{r}, \tag{1}$$

where V is the volume of silicon boxes, $\mathbf{j}(\mathbf{r})$ is the current density of eigenstate field, and $\mathbf{E}e^{ikz}$ represents a normal incidence plane wave with a wave vector k along the z direction and with polarization vector $\mathbf{E}$ in the x-y plane (a unit vector). The integral in Eq. (1) generates the total ED moment of the entire structure. For unperturbed nanostructures such as the original metasurface,

$$c \propto \mathbf{P} \cdot \mathbf{E} = 0 \tag{2}$$

is the condition for ideal symmetry-protected BICs. The symmetry disorders can result in the eigenstate field in the nanostructures coupling to radiative plane waves for x or y polarization. The x and y components of coupling strength can be expressed as:

$$c_{x,y} \propto \mathbf{P} \cdot \mathbf{E}_{x,y} = P_{x,y}. \tag{3}$$

Thus, the zero-order-diffraction quasi-BICs in periodic nanostructures cannot be excited unless the eigenstate near-field generates in-plane ED moment.

The variations of in-plane components of ED moment P_x and P_y as a function of asymmetry parameters p_x, p_y, or δp are depicted in Figs. 4(g)–4(i). For BICs mode M_{A1}, ED moment remains zero when only tuning p_x. The ED moment increases from zero as p_y deviates from 660 nm (the parameter value of the original metasurface), as shown in Fig. 4(g). For mode M_{A2}, the effects of p_x and p_y will exchange, as plotted in Fig. 4(h). For BICs mode M_{B1} [see Fig. 4(i)], a total in-plane ED moment (along the y direction) will not appear unless simultaneously perturbing both asymmetry parameters p_x and p_y. The in-plane EM multipole analyses are in good agreement with Q factor evolution in Figs. 4(a)–4(c) and reflection spectra in Fig. 3. It is worth noting that the overlapping between eigenstate field and the incident light can be applied in structured light (e.g., vector beams) as well, when the coupling strength is attributed to high-order EM multipoles

TABLE I. Symmetry of multiband BICs and broken symmetry elements in quasi-BICs.

BICs modes	Space group	Point group	Irreducible representations	Broken symmetry elements in quasi-BICs
M_{A1}	*pmm*	C_{2v}	B_1	C_2^x
M_{A2}	*pmm*	C_{2v}	B_2	C_2^y
M_{B1}	*pmm*	C_{2v}	A_2	C_2^x, C_2^y
M_{B2}	*pmm*	C_{2v}	B_1	C_2^x
M_{B3}	*pmm*	C_{2v}	B_2	C_2^y

[25]. We also summarize the symmetry of multiband BICs and the broken symmetry elements in quasi-BICs in Table I. The point group and space group of the original metasurface and the perturbed metasurface remain invariant. Due to the intrinsic symmetry distinction (irreducible representations) of ideal BICs, quasi-BICs in the perturbed metasurface are triggered by breaking different symmetry elements (C_2^x or/and C_2^y).

We also propose a sensing method based on the multiband resonances with high-Q factors to distinguish among birefringence refractive indices n_o, n_e, and cladding thickness. The diagram of the proof-of-concept is illustrated in Fig. 5(a). The nanoboxes metasurfaces are covered by an anisotropic medium, which is higher than the nanoboxes by δh. For simplicity, we take uniaxial crystals as an example. Generally, spectral locations and Q factors of resonances are functions of the cladding refractive indices and the thickness, i.e., $\lambda_1(n_o, n_e, \delta h)$, $Q_1(n_o, n_e, \delta h)$, $\lambda_2(n_o, n_e, \delta h)$, $Q_2(n_o, n_e, \delta h)$, etc. Each of the functions is a different sensing channel and supports a different degree of freedom in a sensing problem. The more sensing channels, the more precise sensing would be. To avoid a complicated three-dimensional fitting, we first use dual resonances location channels to sense n_o and n_e, utilizing quasi-BICs mode M_{A1} and M_{B1}. From the 2D fitting plots shown in Figs. 5(b) and 5(c), we can see a well-fitted blue plane to the calculated red dots representing resonance peaks. In Figs. 5(d) and 5(e), we show Q factor linear fitting of refractive indices (n_o, for example) at different cladding thicknesses. The Q factors of BICs modes M_{A1} and M_{B2} are derived through Fano lineshape fitting and are hardly dependent on refractive indices. In contrast, the Q factors vary significantly when modulating the cladding thickness. These results indicate that we could separate cladding thickness (δh) and refractive indices (n_o, n_e) by measuring resonance Q factors. Thus, we can employ the spectral locations and Q factors of multiband quasi-BICs to sense birefringence refractive indices n_o, n_e and the cladding thickness δh, achieving multivariable optical sensing.

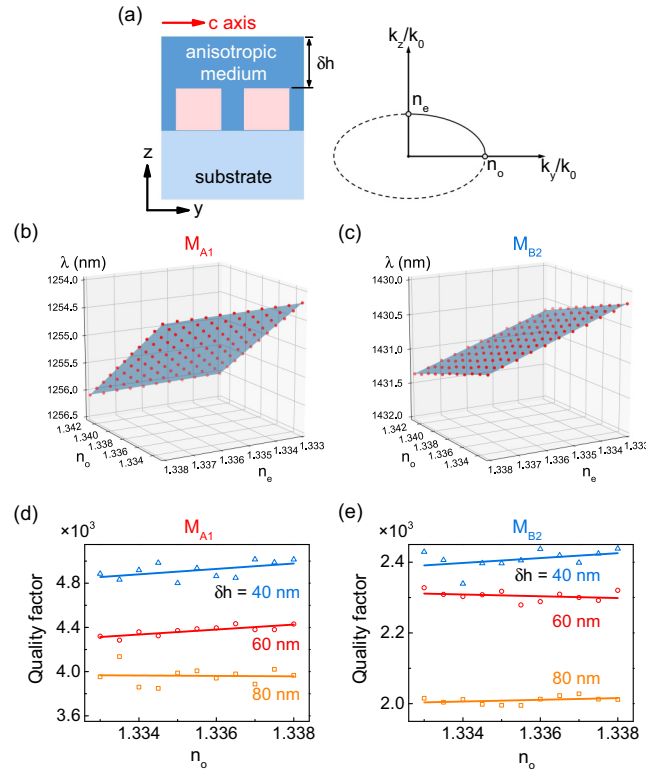

FIG. 5. Birefringence and thickness sensing based on multiband quasi-BICs. (a) The diagram of birefringence sensing, with an anisotropic media (take a uniaxial crystal as an example) on top of the metasurface. We set the optic axis along the y direction. n_o and n_e denote its refractive indices for ordinary light and extraordinary light and the cladding is higher than the nanoboxes by δh. The right panel shows the dispersion relation. (b),(c) Birefringence indices sensing by resonance peak shifts of multiband quasi-BICs. Red dots are locations of resonant peaks from calculated reflection spectra and blue planes are 2D linear fitting results. (d),(e) Thickness sensing by Q factors of quasi-BICs resonances to distinguish cladding thickness and refractive indices. Solid lines are linear fitting of Q factor, which is derived by Fano fitting of reflection spectra. The period p_x is 840 nm and p_y is 680 nm.

IV. CONCLUSION

In conclusion, we propose an approach that can transform symmetry-protected BICs to quasi-BICs by merely breaking specific symmetry elements of nanostructures, namely in-plane half-turns C_2 and mirror axes σ. Instead of breaking symmetry elements and space groups simultaneously, our approach modulate the periods of metasurfaces and introduce a disorder in the size of the unit cell while keeping the space group invariant. Precisely controlling periods of fabricated nanostructures is generally considered to be more convenient and more accurate than tiny defects in meta-atoms, and the Q factor of flat devices is expected to be further improved. Apart from triggering the transition from ideal BICs to quasi-BICs, the perturbation of the periods enlarges the unit cell as well, which enriches the ideal BICs, achieving multiband quasi-BICs. Besides, selective excitation of multiband quasi-BICs is achieved by tuning the asymmetry parameters and is explained by the irreducible representation of eigenstate field. Some works were devoted to generate accidental BICs or Friedrich-Wintgen BICs by nonperiodic structures [2,5,25] and parameter tuning [49]. We elucidated the relationships among symmetry elements, space group symmetry, and the transition from symmetry-protected BICs to quasi-BICs,

which are rarely discussed in the previous works. Based on the multiband high-Q resonances, a precise sensing mechanism is proposed to detect cladding birefringence refractive indices and thickness, achieving multivariable optical sensing that may be applicable for engineering dynamic metasurfaces (e.g., infiltrated by liquid crystals [50]). The proposed scheme can be further expanded to nonlinear and quantum photonics, and benefits applications from giant harmonic generations, low-threshold lasers, biosensing to photonic circuits.

ACKNOWLEDGMENTS

This work was supported by the National Key Research and Development Program of China (2016YFA0301102 and 2017YFA0303800), the National Natural Science Foundation of China for Distinguished Young Scholars (11925403), the National Natural Science Foundation of China (11904183, 11904181, 11974193, 91856101, and 11774186), and the Natural Science Foundation of Tianjin for Distinguished Young Scientists (18JCJQJC45700).

[1] K. Koshelev, A. Bogdanov, and Y. Kivshar, Meta-optics and bound states in the continuum, Sci. Bull. **64**, 836 (2019).

[2] C. W. Hsu, A. D. S. B. Zhen, J. D. Joannopoulos, and M. Soljačić, Bound states in the continuum, Nat. Rev. Mater. **1**, 16048 (2016).

[3] M. Takeichi and S. Murakami, Topological linelike bound states in the continuum, Phys. Rev. B **99**, 035128 (2019).

[4] Y. X. Xiao, G. C. Ma, Z. Q. Zhang, and C. T. Chan, Topological Subspace-Induced Bound State in the Continuum, Phys. Rev. Lett. **118**, 166803 (2017).

[5] A. B. Andrey, L. K. Kirill, V. K. Polina, V. R. Mikhail, A. G. Sergey, F. S. Zarina, B. S. Kirill, S. K. Yuri, and F. L. Mikhail, Bound states in the continuum and Fano resonances in the strong mode coupling regime, Adv. Photonics **1**, 016001 (2019).

[6] K. Koshelev, A. Bogdanov, and Y. Kivshar, Engineering with bound states in the continuum, Opt. Photon. News **31**, 38 (2020).

[7] C. W. Hsu, B. Zhen, J. Lee, S. L. Chua, S. G. Johnson, J. D. Joannopoulos, and M. Soljačić, Observation of trapped light within the radiation continuum, Nature (London) **499**, 188 (2013).

[8] J. Lee, B. Zhen, S. L. Chua, W. J. Qiu, J. D. Joannopoulos, M. Soljačić, and O. Shapira, Observation and Differentiation of Unique High-Q Optical Resonances near Zero Wave Vector in Macroscopic Photonic Crystal Slabs, Phys. Rev. Lett. **109**, 067401 (2012).

[9] Y. Plotnik, O. Peleg, F. Dreisow, M. Heinrich, S. Nolte, A. Szameit, and M. Segev, Experimental Observation of Optical Bound States in the Continuum, Phys. Rev. Lett. **107**, 183901 (2011).

[10] B. Zhen, C. W. Hsu, L. Lu, A. D. Stone, and M. Soljačić, Topological Nature of Optical Bound States in the Continuum, Phys. Rev. Lett. **113**, 257401 (2014).

[11] L. Xu, K. Z. Kamali, L. J. Huang, M. Rahmani, A. Smirnov, R. Camacho-Morales, Y. X. Ma, G. Q. Zhang, M. Woolley, D. Neshev, and A. E. Miroshnichenko, Dynamic nonlinear image tuning through magnetic dipole quasi-BIC ultrathin resonators, Adv. Sci **6**, 1802119 (2019).

[12] Z. J. Liu, Y. Xu, Y. Lin, J. Xiang, T. H. Feng, Q. T. Cao, J. T. Li, S. Lan, and J. Liu, High-Q Quasibound States in the Continuum for Nonlinear Metasurfaces, Phys. Rev. Lett. **123**, 253901 (2019).

[13] M. K. Liu and D. Y. Choi, Extreme Huygens' metasurfaces based on quasi-bound states in the continuum, Nano. Lett. **18**, 8062 (2018).

[14] K. Koshelev, S. Lepeshov, M. K. Liu, A. Bogdanov, and Y. Kivshar, Asymmetric Metasurfaces With High-Q Resonances Governed by Bound States in the Continuum, Phys. Rev. Lett. **121**, 193903 (2018).

[15] J. C. Jin, X. F. Yin, L. F. Ni, M. Soljačić, B. Zhen, and C. Peng, Topologically enabled ultrahigh-q guided resonances robust to out-of-plane scattering, Nature (London) **574**, 501 (2019).

[16] S. I. Azzam, V. M. Shalaev, A. Boltasseva, and A. V. Kildishev, Formation of Bound States in the Continuum in Hybrid Plasmonic-Photonic Systems, Phys. Rev. Lett. **121**, 253901 (2018).

[17] W. Z. Liu, B. Wang, Y. W. Zhang, J. J. Wang, M. X. Zhao, F. Guan, X. H. Liu, L. Shi, and J. Zi, Circularly Polarized States Spawning from Bound States in the Continuum, Phys. Rev. Lett. **123**, 116104 (2019).

[18] C. Huang, C. Zhang, S. M. Xiao, Y. H. Wang, Y. B. Fan, Y. L. Liu, N. Zhang, G. Y. Qu, H. J. Ji, J. C. Han, L. Ge, Y. Kivshar, and Q. Song, Ultrafast control of vortex microlasers, Science **367**, 1018 (2020).

[19] B. Wang, W. Z. Liu, M. X. Zhao, J. J. Wang, Y. W. Zhang, A. Chen, F. Guan, X. H. Liu, L. Shi, and J. Zi, Generating optical vortex beams by momentum-space polarization vortices centred at bound states in the continuum, Nat. Photonics **14**, 623 (2020).

[20] M. Livio, Why symmetry matters, Nature (London) **490**, 472 (2012).

[21] S. K. Ozdemir, S. Rotter, F. Nori, and L. Yang, Parity-time symmetry and exceptional points in photonics, Nat. Mater. **18**, 783 (2019).

[22] X. F. Li, X. Ni, L. A. Feng, M. H. Lu, C. He, and Y. F. Chen, Tunable Unidirectional Sound Propagation through a Sonic-Crystal-Based Acoustic Diode, Phys. Rev. Lett. **106**, 084301 (2011).

[23] K. Koshelev, Y. T. Tang, K. F. Li, D. Y. Choi, G. X. Li, and Y. Kivshar, Nonlinear metasurfaces governed by bound states in the continuum, ACS Photonics **6**, 1639 (2019).

[24] A. S. Kupriianov, Y. Xu, A. Sayanskiy, V. Dmitriev, Y. S. Kivshar, and V. R. Tuz, Metasurface Engineering Through Bound States In The Continuum, Phys. Rev. Appl. **12**, 014024 (2019).

[25] K. Koshelev, S. Kruk, E. Melik-Gaykazyan, J. H. Choi, A. Bogdanov, H. G. Park, and Y. Kivshar, Subwavelength dielectric resonators for nonlinear nanophotonics, Science **367**, 288 (2020).

[26] Y. B. Zhang, W. W. Liu, Z. C. Li, Z. Li, H. Cheng, S. Q. Chen, and J. G. Tian, High-quality-factor multiple Fano resonances for refractive index sensing, Opt. Lett. **43**, 1842 (2018).

[27] M. F. Limonov, M. V. Rybin, A. N. Poddubny, and Y. S. Kivshar, Fano resonances in photonics, Nat. Photonics **11**, 543 (2017).

[28] A. C. Overvig, S. C. Malek, M. J. Carter, S. Shrestha, and N. Yu, Selection rules for quasibound states in the continuum, Phys. Rev. B **102**, 035434 (2020).

[29] N. F. Yu, P. Genevet, M. A. Kats, F. Aieta, J. P. Tetienne, F. Capasso, and Z. Gaburro, Light propagation with phase discontinuities: Generalized laws of reflection and refraction, Science **334**, 333 (2011).

[30] M. V. Rybin, D. S. Filonov, K. B. Samusev, P. A. Belov, Y. S. Kivshar, and M. F. Limonov, Phase diagram for the transition from photonic crystals to dielectric metamaterials, Nat. Commun. **6**, 10102 (2015).

[31] Y. Yang, I. I. Kravchenko, D. P. Briggs, and J. Valentine, All-dielectric metasurface analogue of electromagnetically induced transparency, Nat. Commun. **5**, 5753 (2014).

[32] I. Staude and J. Schilling, Metamaterial-inspired silicon nanophotonics, Nat. Photonics **11**, 274 (2017).

[33] S. Han, S. Kim, S. Kim, T. Low, V. W. Brar, and M. S. Jang, Complete complex amplitude modulation with electronically tunable graphene plasmonic metamolecules, ACS Nano **14**, 1166 (2020).

[34] G. X. Li, S. M. Chen, N. Pholchai, B. Reineke, P. W. H. Wong, E. Y. B. Pun, K. W. Cheah, T. Zentgraf, and S. Zhang, Continuous control of the nonlinearity phase for harmonic generations, Nat. Mater. **14**, 607 (2015).

[35] L. Wang, S. Kruk, K. Koshelev, I. Kravchenko, B. Luther-Davies, and Y. Kivshar, Nonlinear wavefront control with all-dielectric metasurfaces, Nano. Lett. **18**, 3978 (2018).

[36] H. Zhou, B. Sain, Y. Wang, C. Schlickriede, R. Zhao, X. Zhang, Q. Wei, X. Li, L. Huang, and T. Zentgraf, Polarization-encrypted orbital angular momentum multiplexed metasurface holography, ACS Nano **14**, 5553 (2020).

[37] Y. Zhou, H. Zheng, I. I. Kravchenko, and J. Valentine, Flat optics for image differentiation, Nat. Photonics **14**, 316 (2020).

[38] W. W. Liu, D. N. Ma, Z. C. Li, H. Cheng, D. Y. Choi, J. G. Tian, and S. Q. Chen, Aberration-corrected three-dimensional positioning with a single-shot metalens array, Optica **7**, 1706 (2020).

[39] D. N. Maksimov, V. S. Gerasimov, S. Romano, and S. P. Polyutov, Refractive index sensing with optical bound states in the continuum, Opt. Express **28**, 38907 (2020).

[40] F. Yesilkoy, E. R. Arvelo, Y. Jahani, M. K. Liu, A. Tittl, V. Cevher, Y. Kivshar, and H. Altug, Ultrasensitive hyperspectral imaging and biodetection enabled by dielectric metasurfaces, Nat. Photonics **13**, 390 (2019).

[41] S. Romano, G. Zito, S. N. L. Yepez, S. Cabrini, E. Penzo, G. Coppola, I. Rendina, and V. Mocella, Tuning the exponential sensitivity of a bound-state-in-continuum optical sensor, Opt. Express **27**, 18776 (2019).

[42] L. H. Wu and X. Hu, Scheme for Achieving a Topological Photonic Crystal by using Dielectric Material, Phys. Rev. Lett. **114**, 223901 (2015).

[43] E. D. Palik, *Handbook of Optical Constants of Solids* (Academic Press, Orlando, 1985).

[44] M. S. Dresselhaus, G. Dresselhaus, and A. Jorio, *Group Theory: Application to the Physics of Condensed Matter* (Springer-Verlag, Berlin, 2008).

[45] K. Yao and Y. M. Liu, Enhancing circular dichroism by chiral hotspots in silicon nanocube dimers, Nanoscale **10**, 8779 (2018).

[46] G. G. C Tserkezis1 and N. Stefanou1, Optical properties of metasurfaces infiltrated with liquid crystals, J. Phys.: Condens. Matter **20**, 075232 (2008).

[47] J. B. Lassiter, J. Aizpurua, L. I. Hernandez, D. W. Brandl, I. Romero, S. Lal, J. H. Hafner, P. Nordlander, and N. J. Halas, Close encounters between two nanoshells, Nano. Lett. **8**, 1212 (2008).

[48] M. V. Gorkunov, A. A. Antonov, and Y. S. Kivshar, Metasurfaces with Maximum Chirality Empowered by Bound States in the Continuum, Phys. Rev. Lett. **125**, 093903 (2020).

[49] L. J. Yuan and Y. Y. Lu, Parametric dependence of bound states in the continuum on periodic structures, Phys. Rev. A **102**, 033513 (2020).

[50] A. Lininger, A. Y. Zhu, J. S. Park, G. Palermo, S. Chatterjee, J. Boyd, F. Capasso, and G. Strangi, Optical properties of metasurfaces infiltrated with liquid crystals, Proc. Natl. Acad. Sci. USA **117**, 20390 (2020).